AIP | Applied Physics Letters

Dipolar-glass-like relaxor ferroelectric behaviour in the 0.5BaTiO3-0.5Bi(Mg1/2Ti1/2)O3 electroceramic

Jian Wang, Yun Liu, Qian Li, Kenny Lau, Ray L. Withers et al.

Citation: Appl. Phys. Lett. **103**, 042910 (2013); doi: 10.1063/1.4816741
View online: http://dx.doi.org/10.1063/1.4816741
View Table of Contents: http://apl.aip.org/resource/1/APPLAB/v103/i4
Published by the AIP Publishing LLC.

Dipolar-glass-like relaxor ferroelectric behaviour in the $0.5BaTiO_3$-$0.5Bi(Mg_{1/2}Ti_{1/2})O_3$ electroceramic

Jian Wang,[1] Yun Liu,[1,a)] Qian Li,[1] Kenny Lau,[1] Ray L. Withers,[1,a)] Zhenrong Li,[2] and Zhuo Xu[2]
[1]*Research School of Chemistry, The Australian National University, Canberra, ACT 0200, Australia*
[2]*Electronic Materials Research Laboratory (EMRL), Xian Jiaotong University, Shaanxi 710049, China*

(Received 11 February 2013; accepted 5 July 2013; published online 26 July 2013)

In this study, the dielectric and ferroelectric switching behaviour of $0.5BaTiO_3$-$0.5Bi(Mg_{1/2}Ti_{1/2})O_3$ (BT-BMT) ceramics are investigated. The BT-BMT ceramic exhibits a typical dipolar-glass-like, dielectric polarisation relaxation. This is attributed to the 15 distinct possible local A_4B_2 configurations around the O ions and the effect this unavoidable local compositional variability has on the dipole relaxation behaviour of inherent 1-D ⟨111⟩ dipole chains, arising from correlated off-centre displacements of Bi^{3+} and Ti^{4+} ions along local ⟨111⟩ directions. On the other hand, switchable polarisation under strong applied electric fields is observed on different length scales accompanied by the appearance of strong polarisation relaxation, as observed via time-delayed piezoresponse hysteresis loop measurements. These experimental results demonstrate that this BT-BMT ceramic is relaxor ferroelectric in nature, although it exhibits dipolar-glass-like dielectric relaxation behaviour.
 [http://dx.doi.org/10.1063/1.4816741]

$(1-x)BaTiO_3$-$xBi(Mg_{1/2}Ti_{1/2})O_3$ [(1−x)BT-xBMT] ceramics have recently been investigated for potential high temperature capacitor and piezoelectric applications.[1,2] When $x < \sim 0.08$, the ceramics show a long-range ordered, tetragonal ferroelectric (FE) state at room temperature. At higher BMT concentrations ($0.08 \leq x \leq 0.6$), however, this tetragonal structure transforms to a metrically "pseudocubic" solid solution phase.[3,4] The composition range of this "cubic" solid solution phase can be expanded all the way up to $x \sim 0.9$ in (111)-oriented epitaxial BT-BMT films.[5] The temperature dependent dielectric properties of these "cubic" BT-BMT ceramics show clear frequency dispersion, i.e., dipolar-glass-like behaviour.[3,4] The largely temperature-stable dielectric permittivity at high temperature undergoes a low temperature, frequency-dependent drop due to the freezing in of dipolar relaxational degrees of freedom. The dielectric permittivity thus exhibits a one-step increase on increasing temperature and comes to an approximately "flat" plateau region after the temperature T_m, the point corresponding to the maximum in dielectric permittivity. These dispersive dielectric and temperature-dependent characteristics are analogous to glassy relaxor dielectrics, such as the Bi-based pyrochlores,[6–9] KBr-KCN,[10] $Rb_{1-x}(NH_4)_xH_2PO_4$, and $Rb_{1-x}(ND_4)_xD_2PO_4$.[11] They differ, however, from those observed for typical relaxor ferroelectrics, such as $PbMg_{1/3}Nb_{2/3}O_3$[12] and other $BaTiO_3$-based compounds[13–16] where a broad but well defined peak in the dielectric permittivity is observed.[17] There has been no discussion in the literature to date as to the nature or structural origin of this glassy dielectric relaxation behaviour. Wada *et al.*[1] have reported polarisation-field hysteresis loops for BT-BMT ceramics in the "cubic" phase range but their loops are quite slim and clearly unsaturated. The relaxor ferroelectric nature of the BT-BMT ceramics, therefore, still remains unknown.

The purpose of the current paper is to carefully investigate the temperature-dependent dielectric properties of a 0.5BT–0.5BMT, i.e., $(Ba_{1/2}Bi_{1/2})(Ti_{3/4}Mg_{1/4})O_3$ pseudocubic, ceramic sample as well as to model and seek to obtain insight into the mechanism/s underlying the polarisation relaxation behaviour in this material via electron diffraction and bond valence sum (BVS) calculations coupled with piezoresponse (PR) force microscopy (PFM).[18,19]

As expected, the synthesised 0.5BT–0.5BMT sample was single phase and metrically cubic ($a = 4.0129(5)$ Å) at room temperature. Figure 1(a) shows the temperature dependent dielectric constant, $\varepsilon(T)$, and dielectric loss tangent, $\tan\delta(T)$, curves of the as-prepared BT-BMT ceramic measured at different frequencies. Note that the dielectric behaviour is strongly dispersive with the dielectric constant decreasing and the dielectric loss tangent increasing with increasing frequency and that the former displays a broad plateau-like maximum over a large temperature range, analogous to the dielectric properties of glassy relaxor dielectrics.[10,11,20] While it is somewhat difficult to accurately measure the peak in the dielectric constant curves in the plateau region at T_m, it is much easier to measure T_{max}, the temperature corresponding to the well-defined maximas in the dielectric loss tangent curves.

In order to minimize any possible effect of oxygen vacancies on the dielectric constant in the higher temperature range,[21] the as-synthesised BT-BMT sample was heat treated in an O_2 atmosphere at 800 °C for 18 h. Figure 1(b) shows the dielectric spectra of this oxygen atmosphere, heat treated sample. The dielectric constant now drops slightly with increasing temperature above T_m. Nonetheless, the plateau-like character still remains, and over an even wider temperature range. The dielectric loss, especially in the higher temperature range at lower frequencies, significantly decreases.

Figure 1(c) shows a Vogel-Fulcher (solid line) fitting of the relation between T_{max} and frequency extracted from the $\tan\delta(T)$ curves shown in Fig. 1(b). Using the Vogel-Fulcher

a)Authors to whom correspondence should be addressed. Electronic addresses: yliu@rsc.anu.edu.au and withers@rsc.anu.edu.au.

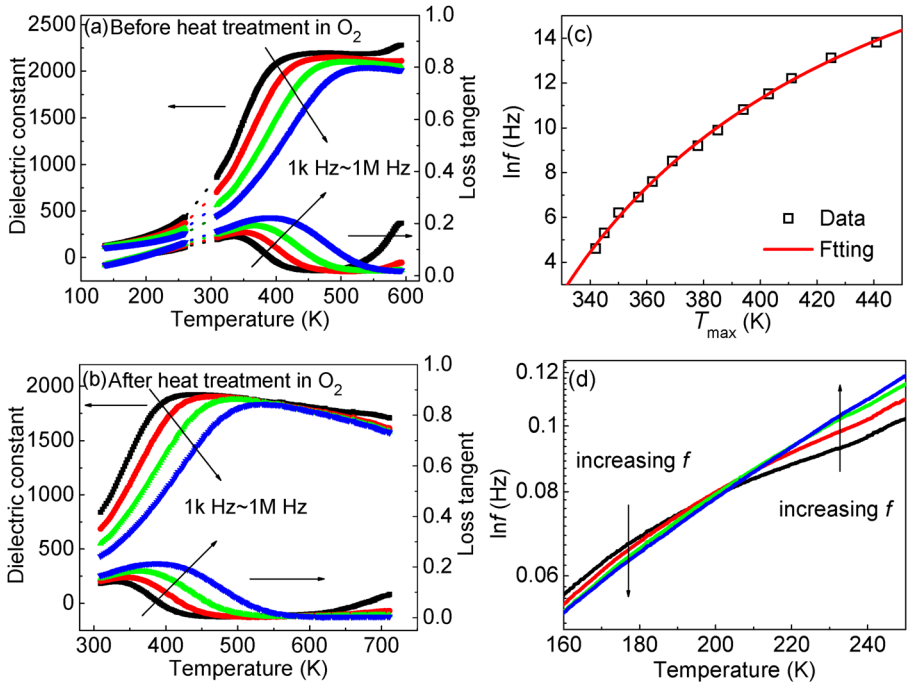

FIG. 1. Temperature dependence of dielectric constant and loss tangent of 0.5BT–0.5BMT ceramic at 1 kHz, 10 kHz, 100 kHz, and 1 MHz (a) before and (b) after heat treatment under O_2 atmosphere, and associated (c) Vogel-Fulcher fittings of T_{max} versus frequency as well as (d) the enlarged loss tangent curves of the BT-BMT ceramic in the temperature range of 160 K to 250 K.

equation $f = f_0 \exp[-E_a/k(T_m - T_f)]$, the experimental data fit very well to the curve obtained using the values $f_0 \sim 1.44 \times 10^{12}$ Hz, $E_a \sim 0.219$ eV and $T_f \sim 213$ K. The freezing frequency f_0 of 1.44×10^{12} Hz is close to typical lattice vibration frequencies (~THz), fixing an upper frequency limit to the relaxational degrees of freedom responsible for the observed dielectric behaviour. The extracted activation energy, E_a, of ~0.219 eV is an order of magnitude larger than for canonical relaxor ferroelectrics[12] but in good agreement with what is observed for the $BaTiO_3$-$BiScO_3$ system. The latter system is a so-called weakly coupled relaxor system,[22] where $BiScO_3$-rich compounds exhibit a similar dipolar-glass-like dielectric relaxation behaviour but ferroelectric behaviour at low temperature. It is interesting to note that the frequency dependence of $\tan\delta$ reverses (Fig. 1(d)) once the temperature is lower than ~210 K, very close to the calculated freezing temperature, T_f.

Given that the freezing frequency and activation energy suggest that the relaxational degrees of freedom responsible for the observed dielectric polarisation relaxation behaviour are intrinsically related to local structure, electron diffraction has been used to search for evidence of the local structural origin of the observed dielectric polarisation. Figures 2(a)–2(c) shows typical room temperature electron diffraction patterns (EDPs) of the 0.5BT–0.5BMT sample along the (a) ⟨100⟩, (b) ⟨111⟩, and (c) ⟨−122⟩ zone axes, respectively. In addition to the well-defined set of parent perovskite Bragg reflections **G**, characteristic transverse polarised {111}* sheets of diffuse intensity are also observed, giving rise to linear diffuse streaking running along the ⟨0,−1,1⟩*, ⟨0,1,−1⟩*, and ⟨011⟩* directions in Figs. 2(a) and 2(b) and along the ⟨4,−1,3⟩* and ⟨4,3,−1⟩* directions in Fig. 2(c).

The fact that this diffuse streaking is transverse polarized requires that the correlated atomic displacements responsible must run largely perpendicular to the {111}* sheets of diffuse intensity, i.e., along the corresponding ⟨111⟩ directions of real space. The sheet-like nature of the diffuse intensity also requires that while these off-centre cation displacements are strongly correlated along ⟨111⟩ (the correlation length is estimated to be ~2–3 nm from the width of the observed diffuse sheets[23]), there is little or no such correlation from one such chain to the next in the transverse direction.

That the ⟨111⟩ off-centre displacement of the Bi^{3+} ions is necessary in the same direction as the off-centred displacement of the Ti^{4+} ions in the same 1-D chain is apparent from the fact that the diffuse streaking passing through $h+k+l$ even parent reflections, such as, e.g., 411 in Fig. 2(c) is always substantially stronger than that passing through $h+k+l$ odd parent reflections, such as, e.g., 210 in Fig. 2(c) (see also Refs. 13, 14, and 23). Fig. 2(d) shows an illustration of the implied 1-D chain dipoles along a particular [111] direction in real space.[13,14,23] Frozen in, largely transverse correlated, $[111]_p$ (subscript p for parent perovskite substructure) chain dipoles of precisely this type are known to be responsible for the rhombohedral ferroelectric phases of the $Pb(Zr_{1-x}Ti_x)O_3$ (PZT) system[24] and $BiFeO_3$.[25]

In order to gain insight into the crystal chemistry underlying the existence of these 1-D ⟨111⟩ nano-scale, dipolar chains as well as for the wide spread in relaxation frequencies associated with the observed dipolar relaxation, bond valence sum calculations[26–29] assuming an ideal undistorted, $a = 4.0129$ Å, $Pm\bar{3}m$ perovskite average structure were carried out. The calculated apparent valences (AVs) of the cations without any off-centre displacements are as follows: $AV(Ba^{2+}) = 2.589$ valence units (vu), $AV(Bi^{3+}) = 1.757$ vu, $AV(Mg^{2+}) = 2.230$ vu, and $AV(Ti^{4+}) = 3.520$ vu. Note that the Ba^{2+} and Mg^{2+} cations are significantly over-bonded whereas the Bi^{3+} and Ti^{4+} cations, in particular the Bi^{3+} cation, are very significantly under-bonded. These results require large amplitude, off-centre displacements of both the Bi^{3+} and Ti^{4+} cations, which of necessity should be locally correlated, i.e., primarily in the same direction, in order to avoid over-bonding of neighbouring oxygen ions. Indeed the under-bonding of the Bi^{3+} ions is so large in the ideal *A* site

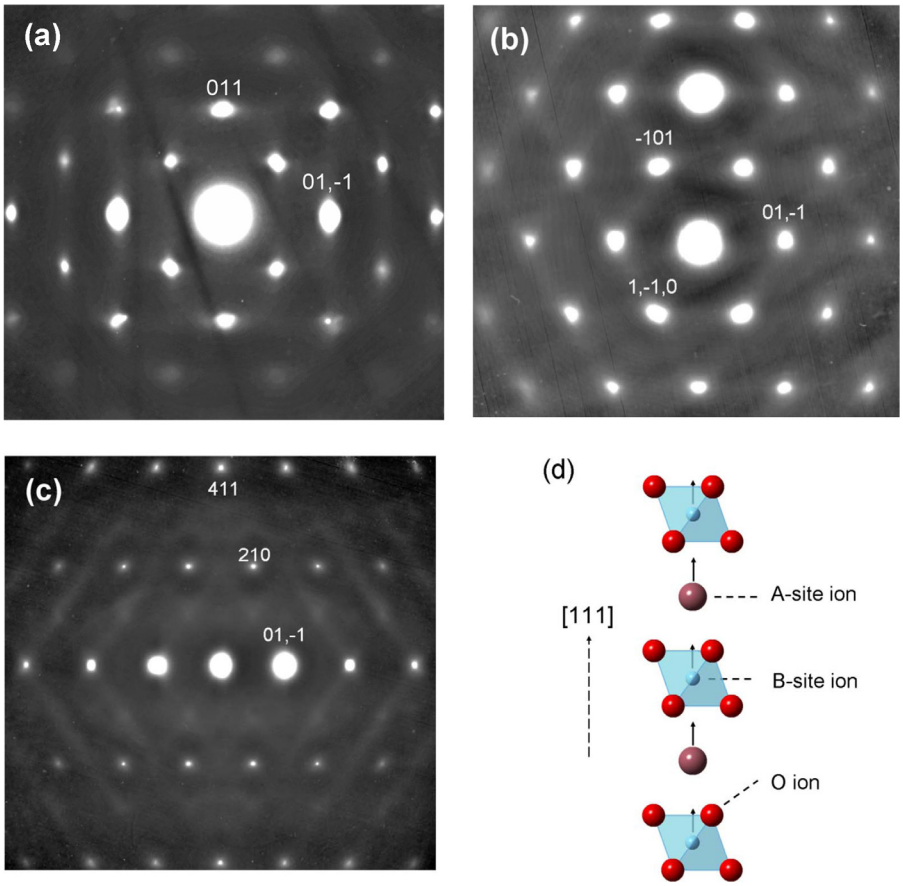

FIG. 2. Electron diffraction patterns collected along the (a) ⟨100⟩, (b) ⟨111⟩, and (c) ⟨−122⟩ zone axes. (d) An illustration of the [111] dipole chains in the "cubic" average structure responsible for the observed structured diffuse distribution. The solid arrows indicate the necessarily in-phase direction of displacement of the *A*-site and *B*-site ions.

position, and the required off-centre displacements of the local Bi^{3+} ions so pronounced, that any resultant dipoles are unlikely to be able to be flipped except under the action of an extremely strong applied electric field. They also strongly suggest that the Ba^{2+} and Mg^{2+} cations will not move off-centre in their local oxygen co-ordination environments.

Taken together, these bond valence results strongly suggest that the nano-scale 1-D ⟨111⟩ dipole chains required by the diffraction evidence result primarily from the large amplitude, correlated off-centre displacements along local ⟨111⟩ directions of Bi^{3+} and Ti^{4+} cations relative to the oxygen ion sub-structure, as shown in Figs. 3(a)–3(d), and are the origin of local polarization in this BT-BMT system. That this is indeed likely to be the case can be seen from Fig. 3 which shows G_{II}^2-minimized[27–29] (G_{II} = the so-called global instability index) local structures derived for various different possible local compositions and assumed space group symmetries, e.g., for $BiTiO_3$ in (a) and (b), for $BiBaTi_2O_6$ in (c) and (d), for $BaTiO_3$ in (e) and for $BiBaMgTiO_6$ in (f). (It has been shown via comparison with discrete Fourier transform (DFT) calculations in several recent papers[27–29] that G_{II}^2 scales to a very good approximation with energy, with a rough scaling constant ∼500 mRy,[27] (or 6.8 eV)/[vu]^2). The associated structural as well as bond valence sum details for all the structures shown in Fig. 3 are given in Ref. 35.

In the case of $BiTiO_3$ (*cf.* Figs. 3(a) and 3(b)), it is intriguing that neighbouring 1-D $[111]_p$ dipole can either be in-phase and thus FE, as in (a), or out-of-phase and antiferroelectric (AFE), as in (b). In either case, the local value for G_{II}^2, or energy,[27–29] reduces very significantly (from the parent value of $(0.604)^2$ to $(0.201)^2$ vu^2) and remains very nearly the same whether FE or AFE, consistent with the observed electron diffraction evidence of ⟨111⟩ sheets of diffuse intensity (see Ref. 35 for details). The same is true for the $BiBaTi_2O_6$ case (cf. Figs. 3(c) and 3(d)), where G_{II}^2, or energy, again reduces significantly from the undisplaced parent value in both the FE and AFE-like cases. This ability to flip the sign of neighbouring [111] dipoles and not incur an energy penalty means that intergrowths of Figs. 3(a) and 3(b), or Figs. 3(c) and 3(d), or mixtures thereof can easily be envisaged and likely underlies the existence of the observed **G** ± {111}* sheets of diffuse intensity (see Fig. 2). In the Ba and/or Mg rich cases of $BaTiO_3$ and $BiBaMgTiO_6$ (Figs. 3(e) and 3(f)), however, the ability to flip the sign of neighbouring [111] dipoles and not incur an energy penalty is no longer true (again, see Ref. 35, for details).

For an example of how the 4 possible (8 when dipolar sign is taken into account) 1-D ⟨111⟩ nano-scale, dipolar chains, ∼2–3 nm in length, implied by the observed diffraction evidence can quite happily co-exist on a larger scale, see, e.g., Figs. 4 and 8 of Ref. 24. Note that the diffuse scattering modelled in Ref. 24 is essentially identical with that shown in Fig. 2 of this paper and that the ordered dipolar chain regions along any one particular ⟨111⟩ direction (shown in Fig. 4 of Ref. 24) co-exist with disordered regions where the local ⟨111⟩ dipole is not along the original ⟨111⟩ direction. Given that 50% of the perovskite *A* site positions must be occupied by a Bi^{3+} ion and 75% of the perovskite *B* site positions must be occupied by a Ti^{4+} ion and that all of these Bi^{3+} and Ti^{4+} ions must undergo large amplitude, off-centre displacements which we assume to be along a local ⟨111⟩ direction, it is not unreasonable to suggest that

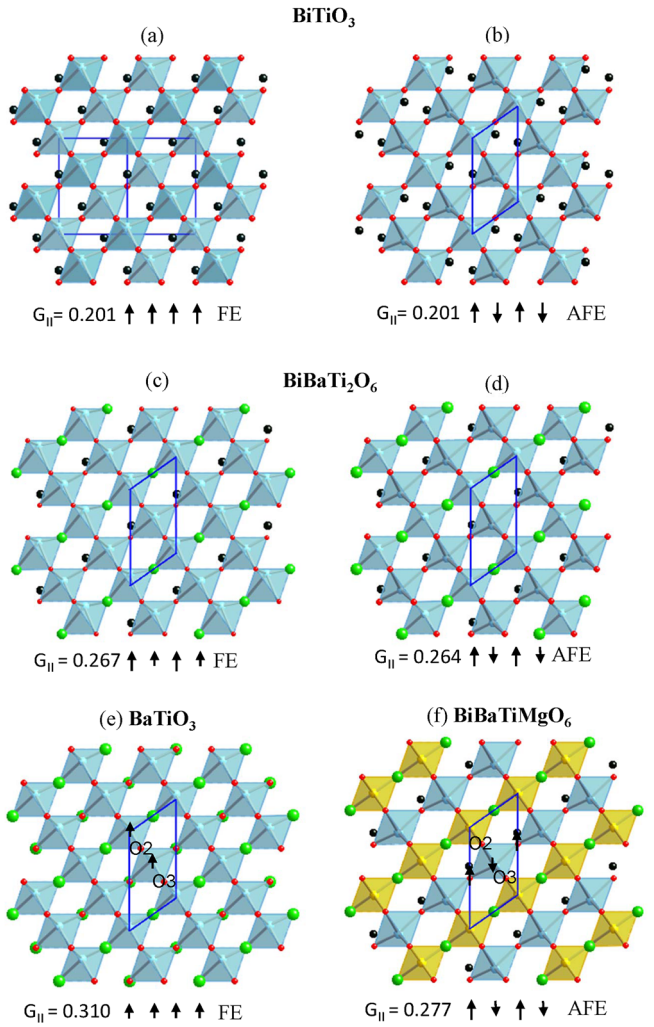

FIG. 3. The local structures derived for a few possible local compositions and assumed space group symmetries for $BiTiO_3$ (a) and (b), $BiBaTi_2O_6$ (c) and (d), $BaTiO_3$ (e), and $BiBaMgTiO_6$ (f) as well as GII value. Arrows are the directions of cation displacements (the line length corresponds to the larger or smaller displacement).

Fig. 4 of Ref. 24 in conjunction with Fig. 3 of this paper provides a highly plausible model of the local ordering and polarization in BT-BMT.

It is clear from the above calculations, given the myriad of distinct possible configurations that can occur (there are 15 compositionally distinct, and 18 crystallographically distinct, possible local A_4B_2 coordination environments surrounding each O^{2-} ion), that the application of the relatively small amplitude applied electric fields involved in dielectric spectroscopy are unlikely to be able to switch the off-centre sign of the local Bi^{3+} displacements. Such a field is much more likely to cause local rotations in the directions of the off-centre Bi and Ti ion displacements and thus of the local polarisation. It may even be possible to rotate from one ⟨111⟩ direction to another. The observed dielectric relaxation behaviour can then be attributed to the many different ways in which the perturbed local dipole polarisations can relax back towards equilibrium. It would not be surprising that these relaxational degrees of freedom would freeze out over a wide range of different temperatures depending upon the exact local stoichiometry, consistent with the observed glass-like dielectric relaxation behaviour.

The above observations strongly suggest the presence of local ⟨111⟩ dipole chains in the BT-BMT sample. Experimentally, however, the macroscopic hysteresis loop is quite slim and still not saturated under an applied electric field of 60 kV/cm (inset in Fig. 4(c)), which makes it difficult to judge the ferroelectric nature, or otherwise, of the sample. PFM and switching spectroscopy PFM measurements were thus conducted to investigate the switching capability of the polarisation. Figures 4(a) and 4(b) show room temperature PFM phase and amplitude images of the sample both before (the bottom part of the image) and after poling (the top part). No ferroelectric domain features are observed in the unpoled sample in either the phase or amplitude images consistent with uncorrelated dipoles on the scale of only a few nanometers. This significantly differs with the behaviour observed in canonical relaxor ferroelectrics[12–15] in which micrometer-scale domains, originating from strongly correlated polar domain clusters, are observable even above T_c.[30,31] After poling, on the other hand, the regions ($1\ \mu m \times 3\ \mu m$) exposed to either a positive (+20 V) or a negative voltage (−20 V) exhibit a similar amplitude image contrast but an ∼180° phase change (see the top parts of Figs. 4(a) and 4(b)), indicating the switchable nature of the induced polarisation within the sample. In addition, switching spectroscopy PFM (∼50 nm scale) enables the measurement of local PR hysteresis loops as well as the superposition of the dynamic behavior of ferroelectric domain nucleation and evolution.[18,19] Such switching spectroscopy PFM characterisation shows typical PR hysteresis loops (Fig. 4(c)) associated with a considerable relaxation behaviour, suggesting the relaxor ferroelectric nature of BT-BMT. Note that the electric field under the PFM tip is rather large (10^6–10^7 V/cm). The low observed macroscopic polarisation can thus be attributed to the relatively low applied electric field and the small scale of transverse correlation of the inherent 1-D dipole chains. Besides, the relatively high

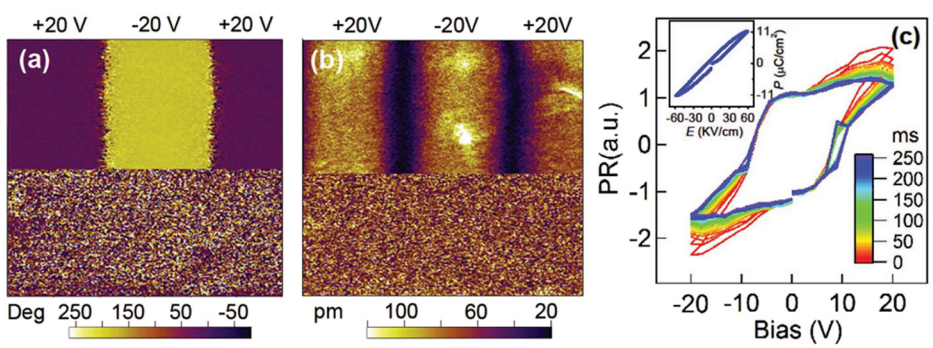

FIG. 4. (a) PFM phase and (b) amplitude images of the surface in a $3 \times 3\ \mu m$ area. The top half parts are for the poled state (poling voltage ±20 V) and the bottom half are for the corresponding unpoled state. (c) Time-delayed hysteresis loops. The inset shows the macroscopic hysteresis loop of the bulk sample.

$\tan\delta$ ($\sim$0.12) of the BT-BMT sample also makes polarisation switching difficult in a bulk sample.

The above PFM observations confirm the ferroelectric nature of the 0.5BT–0.5BMT ceramic under a sufficiently large enough applied electric field to switch/align the local off-centre displacements of the Bi^{3+} and Ti^{4+} ions. The local ordering of the 1-D dipoles is too weak under normal conditions to form macro, or even over a few hundreds of nanometre scale, domains that can be observed using PFM. However, under a sufficiently large applied electric field, the inherent dipole chains are switchable and exhibit a typical PR hysteresis loop character as shown in Fig. 4(c).

It is suggested that the observed dielectric polarisation relaxation arises from the field induced, local off-centre displacements of the Bi^{3+} and Ti^{4+} ions when T is high than T_f. It is widely accepted that the dipoles freeze when the temperature approaches the freezing point T_f,[32–34] in good agreement with our experimental data. When the temperature is lower than T_f, another relaxation mechanism appears, showing a different frequency dependent trend as the temperature varies.

In summary, electron diffraction data from a 0.5BT–0.5BMT ceramic show characteristic $\mathbf{G} \pm \{111\}^*$ sheets of diffuse intensity, consistent with the presence of 1-D $\langle 111 \rangle$ dipole chains along the four $\langle 111 \rangle$ directions of real space. These 1-D dipole chains have a correlation length along the local $\langle 111 \rangle$ chain direction of $\sim$2–3 nm. It is suggested that the myriad of distinct possible local configurations around the O ions leads to a typical dipolar-glass-like dielectric polarisation relaxation. The sample is relaxor ferroelectric in nature, as indicated by the switchable polarisation and typical PR hysteresis loops on different length scales.

The authors J.W., Y.L., and R.L.W. acknowledge the support of the Australian Research Council (ARC) in the form of Discovery projects. Y.L. also appreciates support from the ARC Future Fellowships program.

[1]S. Wada, K. Yamato, P. Pulpan, N. Kumada, B.-Y. Lee, T. Iijima, C. Moriyoshi, and Y. Kuroiwa, J. Appl. Phys. **108**, 094114 (2010).
[2]R. Sun, X. L. Wang, J. Shi, and L. Wang, Appl. Phys. A **104**, 129–133 (2011).
[3]Q. Zhang, Z. R. Li, F. Li, and Z. Xu, J. Am. Ceram. Soc. **94**, 4335–4339 (2011).
[4]B. Xiong, H. Hao, S. J. Zhang, H. X. Liu, and M. H. Cao, J. Am. Ceram. Soc. **94**, 3412–3417 (2011).
[5]H. Tanaka, M.-T. Chentir, T. Yamada, S. Yasui, Y. Ehara, K. Yamato, Y. Kashiwagi, C. N. Theng, J. Wang, S. Okamura *et al.*, J. Appl. Phys. **111**, 084108 (2012).
[6]R. L. Withers, T. R. Welberry, A.-K. Larsson, Y. Liu, L. Norén, H. Rundlöf, and F. J. Brink, J. Solid State Chem. **177**, 231–244 (2004).
[7]W. Somphon, V. Ting, Y. Liu, R. L. Withers, Q. Zhou, and B. J. Kennedy, J. Solid State Chem. **179**, 2495–2505 (2006).
[8]Y. Liu, R. L. Withers, T. R. Welberry, H. Wang, and H. Du, J. Solid State Chem. **179**, 2141–2149 (2006).
[9]B. Nguyen, Y. Liu, and R. L. Withers, J. Solid State Chem. **180**, 549–557 (2007).
[10]N. O. Birge, Y. H. Jeong, S. R. Nagel, S. Bhattacharya, and S. Susman, Phys. Rev. B **30**, 2306–2308 (1984).
[11]P. He, K. Deguchi, M. Hirokane, and E. Nakamura, J. Phys. Soc. Jpn. **59**, 1835–1840 (1990).
[12]D. Viehland, S. J. Jang, L. E. Cross, and M. Wuttig, J. Appl. Phys. **68**, 2916–2921 (1990).
[13]Y. Liu, R. L. Withers, X. Y. Wei, and J. F. Gerald, J. Solid State Chem. **180**, 858–865 (2007).
[14]Y. Liu, R. L. Withers, B. Nguyen, and K. Elliot, Appl. Phys. Lett. **91**, 152907 (2007).
[15]R. L. Withers, Y. Liu, P. Woodward, and Y.-I. Kim, Appl. Phys. Lett. **92**, 102907 (2008).
[16]S. Miao, J. Pokormy, U. M. Pasha, O. P. Thakur, D. C. Sinclair, and I. M. Reaney, J. Appl. Phys. **106**, 114111 (2009).
[17]A. A. Bokov and Z. G. Ye, J. Mater. Sci. **41**, 31–53 (2006).
[18]S. Jesse, A. P. Baddorf, and S. V. Kalinin, Appl. Phys. Lett. **88**, 062908 (2006).
[19]Q. Li, Y. Liu, R. L. Withers, Y. Wan, Z. Li, and Z. Xu, J. Appl. Phys. **112**, 052006 (2012).
[20]V. Bobnar, J. Holc, M. Hrovat, and M. Kosec, J. Appl. Phys. **101**, 074103 (2007).
[21]Y. Gonzalez-Abreu, A. Pelaiz-Barranco, E. B. Araujo, and A. Franco, Jr., Appl. Phys. Lett. **94**, 262903 (2009).
[22]H. Ogihara, C. A. Randall, and S. Trolier-McKinstry, J. Am. Ceram. Soc. **92**, 110–118 (2009).
[23]V. Krayzman and I. Levin, J. Appl. Crystallogr. **45**, 106–112 (2012).
[24]T. R. Welberry, D. J. Goossens, R. L. Withers, and K. Z. Baba-Kishi, Metall. Mater. Trans. A **41**, 1110–1118 (2010).
[25]A. Reyes, C. de la Vega, M. E. Fuentes, and L. Fuentes, J. Eur. Ceram. Soc. **27**, 3709–3711 (2007).
[26]St. Adams, Acta Crystallogr., Sect. B: Struct. Sci. **57**, 278–287 (2001); see also http://www.softbv.net/ for an introduction to bond valence sum calculations.
[27]I. Etxebarria, J. M. Perez-Mato, A. Garcia, P. Blaha, K. Schwarz, and J. Rodriguez-Carvajal, Phys. Rev. B **72**, 174108 (2005).
[28]J. M. Perez-Mato, P. Blaha, K. Schwarz, M. Aroyo, D. Orebengoa, I. Etxebarria, and A. Garcia, Phys. Rev. B **77**, 184104 (2008).
[29]J. M. Perez-Mato, R. L. Withers, A.-K. Larsson, D. Orebengoa, and Y. Liu, Phys. Rev. B **79**, 064111 (2009).
[30]V. V. Shvartsman and A. L. Kholkin, Phys. Rev. B **69**, 014102 (2004).
[31]V. V. Shvartsman and A. L. Kholkin, J. Appl. Phys. **101**, 064108 (2007).
[32]R. Pirc and R. Blinc, Phys. Rev. B **76**, 020101 (2007).
[33]A. A. Bokov and Z.-G. Ye, J. Phys.: Condens. Matter. **12**, L541 (2000).
[34]A. Loidl, Annu. Rev. Phys. Chem. **40**, 29–60 (1989).
[35]See supplementary material at http://dx.doi.org/10.1063/1.4816741 for the associated structural as well as bond valence sum details.